separations

MDPI

Article

Struvite Biomineralization and Phosphorus Recovery by Immobilized *Bacillus velezensis* Using Seawater as the Magnesium Source

Lei Meng [1] and Bin Lian [2,*]

[1] College of Life Science, Nanjing Normal University, Nanjing 210023, China; meng_lei@njnu.edu.cn
[2] Jiangsu Key Laboratory of Ocean-Land Environmental Change and Ecological Construction, College of Marine Science and Engineering, Nanjing Normal University, Nanjing 210023, China
* Correspondence: bin2368@vip.163.com

Abstract

Seawater is rich in Mg^{2+} and can serve as an alternative magnesium source for struvite biomineralization, facilitating phosphorus recovery from aqueous systems. However, the complex ionic conditions can limit the stable metabolism and reuse of free microorganisms. In this study, *Bacillus velezensis* LB002 was immobilized to establish a reusable struvite biomineralization system using seawater as the magnesium source. Its mineralization performance, reusability, and the resource utilization potential of the recovered mineral were evaluated. Immobilized LB002 continuously metabolized nitrogen-containing organic compounds, promoted NH_4^+ accumulation and alkalization, and induced the formation of struvite. In the initial cycle, total phosphorus (TP) removal, phosphorus recovery, and struvite yield reached 98.26%, 54.72%, and 1.43 g/L, respectively. After three consecutive reuse cycles, these values remained at 95.84%, 50.06%, and 1.31 g/L, indicating stable biomineralization performance during repeated operation. Partial breakage of the immobilized bacterial microspheres occurred after the third cycle, while mineralization efficiency remained high, suggesting that carrier mechanical stability may limit longer-term operation. The recovered struvite exhibited a mesoporous structure with a specific surface area of 168.71 m^2/g and a maximum Cd^{2+} adsorption capacity of 446.43 mg/g. Overall, the results demonstrate the feasibility of repeated phosphorus mineralization and recovery using reusable immobilized bacterial microspheres and seawater as the magnesium source under controlled laboratory conditions.

Keywords: struvite biomineralization; seawater as the magnesium source; immobilized microorganisms; phosphorus recovery; Cd^{2+} immobilization

Check for updates

Academic Editor: Shaoping Tong

Received: 27 September 2026
Revised: 14 October 2026
Accepted: 17 October 2026
Published: 20 October 2026

Copyright: © 2026 by the authors. Licensee MDPI, Basel, Switzerland. This article is an open access article distributed under the terms and conditions of the Creative Commons Attribution (CC BY) license.

1. Introduction

Excessive inputs of nitrogen and phosphorus have resulted in widespread eutrophication, which has become a major environmental challenge in lakes, estuaries, and coastal waters [1–3]. Meanwhile, phosphorus resources are finite and non-renewable, and phosphorus recovery from nutrient-rich waters provides dual benefits for pollution control and resource recycling [4]. Therefore, efficiently separating dissolved phosphorus from aqueous systems and converting it into stable, recoverable products is an important strategy for sustainable phosphorus pollution control. Struvite ($MgNH_4PO_4 \cdot 6H_2O$) formation enables the simultaneous recovery of magnesium, ammonium, and phosphorus, converting aqueous

phosphorus into easily separable solid minerals through crystallization. Moreover, the recovered struvite can be further utilized as a slow-release fertilizer or functional material, making it a promising phosphorus recovery product with high resource utilization potential [5,6].

Struvite formation generally requires sufficient supplies of Mg^{2+}, NH_4^+, and PO_4^{3-}, as well as an alkaline environment. Although nitrogen- and phosphorus-containing wastewaters can provide some of the required reactants, Mg^{2+} is often insufficient. Therefore, conventional struvite recovery processes typically require the addition of soluble magnesium salts, such as $MgCl_2$ and $MgSO_4$, increasing operational costs [5,7]. Seawater contains abundant and readily available Mg^{2+}, making it a promising low-cost alternative magnesium source [6]. Direct use of Mg^{2+} from seawater for struvite formation can reduce the demand for commercial magnesium salts and integrate phosphorus separation and resource recovery into a single biomineralization process. However, natural seawater exhibits high ionic strength and contains various competing ions, such as Ca^{2+} and SO_4^{2-}, which may influence microbial metabolism and mineral crystallization. Our previous study demonstrated that *Bacillus velezensis* LB002 maintained metabolic activity in a culture system prepared with natural seawater and utilized Mg^{2+} from seawater to induce the formation of high-purity struvite [6]. Therefore, microbially driven struvite biomineralization using seawater-derived magnesium is feasible under laboratory conditions.

However, free microorganisms are directly exposed to the complex ionic environment of wastewater, where coexisting ions, heavy metals, and other components may affect microbial metabolism and activity. Moreover, their dispersed growth state in reaction systems increases the difficulty of cell separation and recovery, thereby limiting repeated utilization and continuous operation. Immobilization technology can confine microorganisms within matrices possessing sufficient mechanical strength and porous structures, thereby providing cells with a relatively stable local microenvironment and enhancing the recoverability and reusability of the biological units [8–10]. Previous studies have also demonstrated that immobilized bacteria can participate in struvite biomineralization, including comparative investigations of free and immobilized *Bacillus cereus* [8]. Building on these studies, the present work further extends our previously established single-batch free-cell LB002–seawater biomineralization system to a recoverable and reusable immobilized format, with particular emphasis on evaluating phosphorus removal, phosphorus recovery, and biomineralization stability over repeated reuse cycles.

Accordingly, this study immobilized LB002 using an activated carbon–polyvinyl alcohol–sodium alginate composite carrier and investigated the metabolic and biomineralization behaviors of immobilized LB002 under seawater conditions. The structural characteristics and surface properties of the resulting struvite, as well as the stability of phosphorus removal and mineral formation during consecutive reuse of the immobilized microspheres, were also evaluated. In addition, the Cd^{2+} immobilization performance of the recovered struvite was assessed using Cd^{2+} as a representative heavy metal. This study aimed to evaluate whether immobilized LB002 could sustain struvite formation and phosphorus recovery over multiple reuse cycles and to further assess the Cd^{2+} immobilization potential of the recovered mineral under the tested experimental conditions. The findings provide a basis for subsequent evaluation of the applicability of this laboratory-scale culture system in actual eutrophic waters.

2. Materials and Methods

The overall experimental workflow is illustrated in Figure 1. Immobilized bacterial microspheres were first prepared and subsequently used for struvite biomineralization with natural seawater serving as the Mg^{2+} source. At the end of each cultivation cycle, the immobilized microspheres were recovered, washed, and transferred into fresh medium for

the next repeated-batch cycle, whereas the resulting precipitates were collected separately for mineralogical characterization and subsequent Cd^{2+} immobilization experiments.

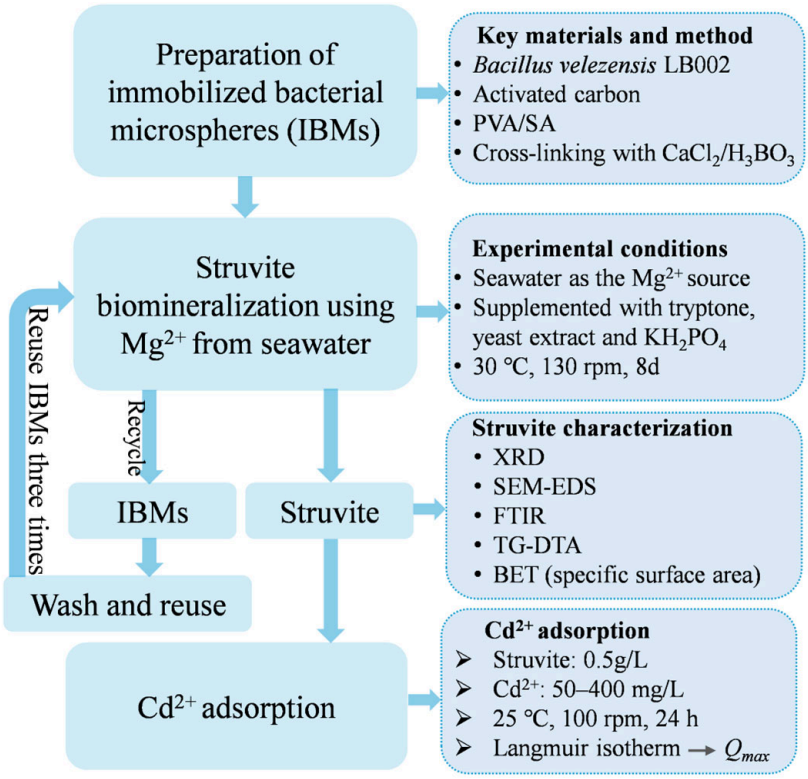

Figure 1. Schematic diagram of the experimental framework.

2.1. Chemicals and Reagents

Tryptone and yeast extract were purchased from Oxoid Ltd. (Basingstoke, UK). Sodium chloride (NaCl), calcium chloride ($CaCl_2$), potassium dihydrogen phosphate (KH_2PO_4), and cadmium chloride ($CdCl_2 \cdot 5/2H_2O$) were obtained from Sinopharm Chemical Reagent Co., Ltd. (Shanghai, China). Polyvinyl alcohol (PVA) was purchased from Aladdin Biochemical Technology Co., Ltd. (Shanghai, China), and sodium alginate (SA) was obtained from Shanghai Macklin Biochemical Co., Ltd. (Shanghai, China). Boric acid (H_3BO_3) was purchased from Sangon Biotech (Shanghai) Co., Ltd. (Shanghai, China). All reagents were of analytical grade.

2.2. Bacterial Strain and Cultivation

The bacterial strain used in this study was *Bacillus velezensis* LB002, whose whole-genome sequence has been deposited in GenBank under accession number CP037417.

The activated LB002 strain was inoculated into 100 mL of sterilized Luria–Bertani (LB) medium. The medium contained 1.0 g of tryptone, 0.5 g of yeast extract, and 1.0 g of NaCl. The culture was incubated at 30 °C with shaking at 130 rpm for 12 h until reaching the logarithmic growth phase. The resulting culture was used as the bacterial inoculum for subsequent immobilization experiments, with a cell density of approximately 4.7×10^9 CFU/mL.

2.3. Preparation of Immobilized Bacterial Microspheres

The immobilization procedure was adapted from previously reported methods [8,10,11]. Activated carbon was used as the bacterial carrier, while polyvinyl alcohol (PVA) and sodium alginate (SA) served as encapsulation materials, with $CaCl_2$ and H_3BO_3 used as cross-linking agents. Briefly, activated carbon was ground and passed through a 100-mesh

sieve, and 0.1 g of the resulting powder was collected. Meanwhile, 0.5 g of PVA and 2.0 g of SA were dissolved in 80 mL of distilled water and continuously stirred in a 95 °C water bath until a viscous solution was obtained. The activated carbon and PVA/SA solution were separately sterilized at 115 °C for 30 min and cooled to room temperature before use. A 100 mL LB002 culture grown to $OD_{600} = 1$ was centrifuged to remove the supernatant. The collected cells were washed three times with sterile water and resuspended in 20 mL of sterile water. The cell suspension was then mixed with activated carbon and incubated with shaking at 30 °C and 130 rpm for 20 min to facilitate cell adsorption onto the carrier. Subsequently, the bacteria-activated carbon mixture was slowly added to the cooled PVA–SA solution and thoroughly mixed. The resulting suspension was then transferred dropwise using a sterile 10 mL syringe into a sterilized cross-linking solution containing 2% $CaCl_2$ and 1% H_3BO_3. The mixture was cross-linked at 4 °C for 8 h to form immobilized bacterial microspheres (IBMs) (Figure S1a). Blank immobilized microspheres were prepared using the same procedure without bacterial cells and used as controls. After cross-linking, the prepared microspheres were rinsed three times with sterile water and stored in 0.9% NaCl solution until further use. The N_2 adsorption–desorption isotherm and pore size distribution of activated carbon are shown in Figure S1b,c.

2.4. Immobilized Bacteria-Induced Struvite Synthesis

Seawater was collected from the Yellow Sea coastal area of Yancheng, Jiangsu Province, China, and filtered through a 0.45 μm membrane to remove suspended impurities. The seawater was subsequently used to prepare the biomineralization medium containing 10.0 g tryptone, 5.0 g yeast extract, 0.4080 g KH_2PO_4, and 1.0 L seawater. The medium was sterilized at 115 °C for 30 min. The basic chemical composition of the seawater is provided in Table S1. The IBMs were added to the medium at 1% (v/v), and their volume was determined using the water displacement method based on the change in water volume before and after adding a known number of IBMs. According to this calculation, 1% (v/v) corresponded to approximately 20 microspheres per 100 mL of culture medium. The cultures were then incubated at 30 °C and 130 rpm for 8 d. In parallel, blank immobilized microspheres without bacterial cells were added to the medium at the same ratio as the control. After incubation, the culture broth was allowed to stand at room temperature for 1 h to facilitate natural sedimentation, and the precipitates at the bottom of the flask were collected. The collected precipitates were thoroughly washed with distilled water and absolute ethanol, dried at 50 °C, and then ground and passed through a 100-mesh sieve for subsequent analyses. All experiments were conducted with three independent replicates.

2.5. Reuse of Immobilized Bacterial Microspheres

After each 8 d biomineralization cycle, the IBMs were recovered from the culture system, washed three times with sterile distilled water, and directly transferred into fresh seawater-based biomineralization medium for the subsequent cycle. The same cultivation conditions were applied in each reuse cycle. The repeated-batch operation was continued until visible structural breakage of the IBMs was observed, at which point the reuse experiment was terminated. Struvite yield, percent removal of total phosphorus (TP), percent recovery of TP, and Mg^{2+} conversion efficiency were determined for each cycle to evaluate the biomineralization stability of the immobilized system during repeated operation.

2.6. Cd^{2+} Adsorption Experiments

Previous studies have shown that Cd^{2+} isothermal adsorption onto biogenic struvite can be well described by the Langmuir model (Equation (1)), which can also be used to estimate the maximum adsorption capacity (Q_{max}) of adsorbent materials [6,12]. Accordingly, Cd^{2+}

adsorption experiments were conducted using solutions prepared from $CdCl_2 \cdot 5/2H_2O$. Recovered struvite was added at 0.5 g/L to Cd^{2+} solutions with initial concentrations ranging from 50 to 400 mg/L, and the mixtures were shaken in centrifuge tubes at 25 °C and 100 rpm for 24 h. The relatively high Cd^{2+} concentrations were selected to provide a sufficiently broad isotherm range and approach saturation of the available adsorption sites. Blank controls without the addition of struvite were run in parallel under identical conditions. After equilibration, the residual Cd^{2+} concentration in solution was determined by flame atomic absorption spectrometry (AAS; AA-6300C, Shimadzu Corporation, Kyoto, Japan). All experiments were performed with three independent replicates. The experimental data were fitted using the Langmuir model to estimate the Q_{max} of the struvite produced in this study, which was subsequently compared with the Cd^{2+} adsorption capacities of previously reported adsorbent materials. The equilibrium adsorption capacity of struvite for Cd^{2+} was calculated using Equation (2) [12].

$$\frac{C_e}{Q_e} = \frac{C_e}{Q_{max}} + \frac{1}{Q_{max}K_L} \quad (1)$$

$$Q_e = \frac{C_0 - C_e}{M} \times V \quad (2)$$

In the equations, C_e represents the equilibrium concentration of Cd^{2+} in solution (mg/L); Q_e represents the adsorption capacity at equilibrium (mg/g); Q_{max} represents the maximum adsorption capacity predicted by the Langmuir model (mg/g); K_L represents the Langmuir constant (L/mg); C_0 represents the initial Cd^{2+} concentration in solution (mg/L); V represents the volume of adsorption solution (L); and M represents the amount of struvite added (g).

2.7. Analytical Parameters and Methods

2.7.1. Analysis of Liquid Phase Indicators

During cultivation, liquid samples were collected periodically to determine pH, OD_{600}, $NH_4{}^+$, TP, and Mg^{2+} concentrations. The pH was measured using a pH meter (PHSJ-4F, Shanghai INESA Scientific Instrument Co., Ltd., Shanghai, China). Liquid-phase OD_{600} was measured using a spectrophotometer (V-5000, Shanghai Metash Instruments Co., Ltd., Shanghai, China) and was primarily used as an operational indicator of cells released from the IBMs and subsequently proliferating in the culture medium rather than as a measure of the total biomass retained within the microspheres. Before the determination of $NH_4{}^+$, TP, and Mg^{2+}, the culture samples were first centrifuged at 11,200× *g* for 5 min. The resulting supernatants were then filtered through 0.22 μm membrane filters prior to chemical analysis. The concentrations of $NH_4{}^+$ and TP were determined using the phenol-hypochlorite method and ammonium molybdate spectrophotometric method, respectively [13]. The percent removal and recovery of TP were calculated using Equations (3) and (4), respectively.

$$\text{Percent removal of TP}(\%) := \frac{[TP]_{Initial} - [TP]_{Residual}}{[TP]_{Initial}} \times 100\% \quad (3)$$

$$\text{Percent recovery of TP}(\%) := \frac{\left[PO_4^{3-}\right]_{Mineral}}{[TP]_{Initial}} \times 100\% \quad (4)$$

The concentration of Mg^{2+} was determined using AAS. To estimate Mg^{2+} transformation efficiency, the minor uptake of Mg^{2+} by microbial cells during cultivation was neglected, and the decrease in Mg^{2+} concentration in the culture medium was considered equivalent to

its conversion into precipitated minerals. The Mg^{2+} transformation efficiency was calculated using Equation (5).

$$\text{Transformation efficiency of } Mg^{2+}(\%) := \frac{\left[Mg^{2+}\right]_{Initial} - \left[Mg^{2+}\right]_{Residual}}{\left[Mg^{2+}\right]_{Initial}} \times 100\% \quad (5)$$

2.7.2. Characterization of Precipitates

The mineral composition of the precipitates was analyzed using an X-ray diffractometer (XRD; D8 Advance, Bruker AXS GmbH, Karlsruhe, Germany). The XRD patterns were collected over a scanning range of 5–90° with a step size of 0.02° and a scanning rate of 5°/min. The crystalline phases were identified using MDI Jade 6.0, and Rietveld refinement of the XRD patterns was performed using GSAS-II 5.6.0 software [14]. The morphology and elemental composition of the minerals were characterized by scanning electron microscopy (SEM; Sigma 300, Carl Zeiss Microscopy GmbH, Oberkochen, Germany) and energy-dispersive spectroscopy (EDS; Xplore30, Oxford Instruments, Abingdon, UK), respectively. Fourier-transform infrared spectroscopy (FTIR; Vertex 70, Bruker Optics GmbH & Co. KG, Ettlingen, Germany) was used to identify mineral structures and organic functional groups. Thermogravimetric–differential thermal analysis (TG-DTA; STA 7300, Hitachi High-Tech, Tokyo, Japan) was performed to evaluate the thermal decomposition characteristics of the samples from 25 to 800 °C at a heating rate of 10 °C/min. The specific surface area and pore size distribution of the minerals were determined using a surface area and pore size analyzer (BET; ASAP 2460, Micromeritics Instrument Corporation, Norcross, GA, USA).

3. Results and Discussion

3.1. Cell Release and Culture-Medium Alkalization During Biomineralization

After the addition of IBMs into the seawater-based biomineralization medium, the OD_{600} values in the liquid phase exhibited a clear time-dependent pattern (Figure 2a). In contrast, the culture medium containing blank immobilized microspheres remained clear throughout the incubation period, with no obvious bacterial proliferation observed. During the initial stage of cultivation, the OD_{600} value increased rapidly and reached a relatively high level on day 2, followed by a relatively stable phase from day 3 to day 8, with a maximum value of 5.19. In our previous study, free LB002 cultured under the same medium composition, cultivation conditions, and sampling schedule exhibited a maximum OD_{600} value of 4.23 [6]. Changes in liquid-phase OD_{600} primarily reflect cells released from the IBMs into the culture medium and subsequently proliferating, rather than the total biomass retained within the immobilized microspheres. In addition, fine suspended mineral particles formed during the later stages of cultivation may also interfere with OD_{600} measurements through light scattering. Therefore, OD_{600} was used in this study only as an auxiliary indicator of changes in liquid-phase cells and was not used to directly infer the effects of immobilization on bacterial growth or salt tolerance. In this system, the immobilized microspheres mainly functioned as recoverable and reusable biological units, providing cells with a relatively stable local microenvironment and continuing to participate in struvite biomineralization during subsequent repeated-batch cycles.

Along with changes in cellular activity, the pH of the culture medium gradually increased from an initial value of approximately 6.8 to approximately 8.1 on day 2 and remained above 9.0 from day 6 to day 8 (Figure 2a). Meanwhile, the NH_4^+ concentration increased rapidly and remained at a relatively high level during the middle and late stages of cultivation (Figure 2b). LB002 can utilize nitrogen-containing organic compounds in the medium,

leading to NH_4^+ accumulation and an increase in pH [6,15]. The accumulation of NH_4^+ and the increase in culture-medium pH indicate that, in cultures containing IBMs, LB002-mediated metabolism of nitrogen-containing organic compounds continuously established alkaline conditions favorable for struvite crystallization. However, the present study cannot quantitatively distinguish the relative contributions of cells retained within the microspheres and those released into the liquid phase to this process.

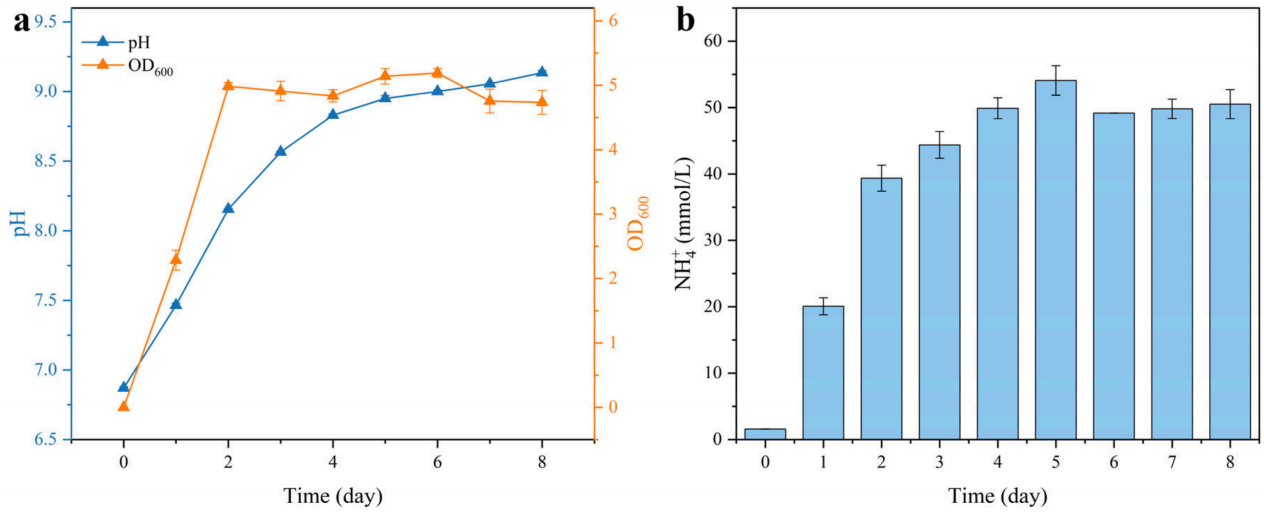

Figure 2. Temporal variations in (**a**) the proliferation dynamics of bacteria released from immobilized bacterial microspheres and pH changes, and (**b**) NH_4^+ concentration during immobilized bacteria-induced biomineralization.

3.2. Mineralogical Characteristics of Struvite

3.2.1. X-Ray Diffraction Analysis

The main diffraction peaks of the precipitates induced by immobilized LB002 were consistent with the standard struvite pattern (PDF#71-2089) (Figure 3). Further Rietveld refinement yielded R_{wp} = 11.42%, R_{exp} = 10.65%, and *GOF* = 1.15, indicating a good agreement between the experimental diffraction pattern and the structural model and confirming that the mineralization products were predominantly struvite with high crystalline-phase purity [16]. Although natural seawater contains Ca^{2+} and other ions that may participate in competitive precipitation in addition to Mg^{2+}, no obvious additional crystalline mineral phases were detected by XRD. This result indicates that high-purity struvite could form under the tested conditions in cultures containing IBMs. This result is consistent with the previous observation of high-purity struvite formation in the free LB002 seawater-based system [6], suggesting that bacterial immobilization did not disrupt the original seawater-derived magnesium struvite biomineralization pathway. Differences were observed between the relative intensities of some crystal planes and those of the standard pattern, with a relatively higher intensity of the (022) plane, suggesting the presence of preferential crystal orientation. During biomineralization, organic molecules and interfacial adsorption may influence the relative growth rates of different crystal planes [17]. In addition, the high concentration of Mg^{2+} in seawater may provide favorable conditions for directional crystal growth along specific orientations [18], contributing to the observed orientation preference. However, variations in relative XRD peak intensities alone are insufficient to elucidate specific bio-interfacial regulatory mechanisms. These results only suggest the possible occurrence of preferential crystal growth under immobilized bacterial mineralization conditions and cannot be directly attributed to the regulation of specific crystal planes by particular biomolecules.

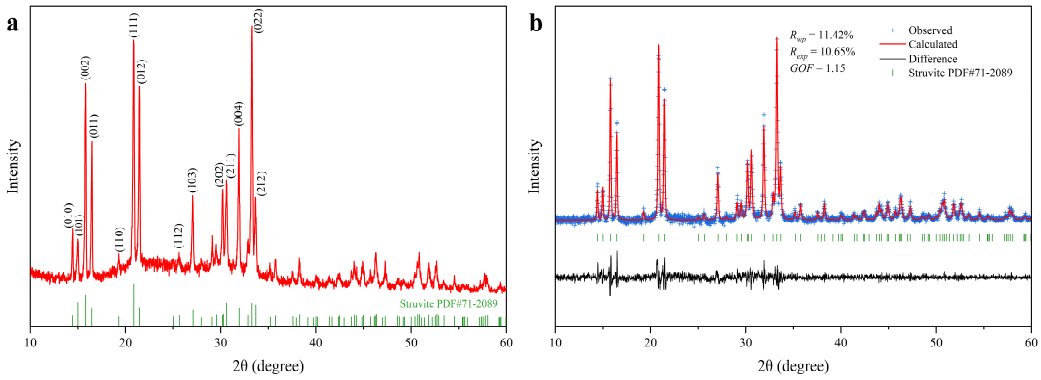

Figure 3. XRD patterns (**a**) and Rietveld refinement results (**b**) of minerals formed during biomineralization with immobilized bacteria. In (**a**), the red line represents the experimental XRD pattern, and the green bars indicate the reference diffraction peaks of struvite (PDF#71-2089).

3.2.2. SEM-EDS Analysis

The morphology of precipitate crystals induced by immobilized bacteria is shown in Figure 4a–c. SEM observations revealed that the mineralization products were mainly composed of elongated and prismatic crystals, with morphologies consistent with typical struvite crystal characteristics [19,20]. Bacteria-like structures and attached organic materials were observed on the surfaces of some crystals (Figure 4b), indicating that cells released from the IBMs and their extracellular products could accumulate on mineral surfaces, forming distinct bio-organic coatings. EDS mapping showed that Mg, P, N, and O were relatively uniformly distributed within the well-developed crystal regions, consistent with the elemental composition of struvite (Figure S2). C and Ca signals were also detected on some crystal surfaces, with Ca signals mainly co-localized with C-rich regions, whereas no obvious Ca enrichment was observed in the regular struvite crystal regions. Combined with the absence of detectable Ca-containing crystalline phases in the XRD patterns, these results suggest that seawater-derived Ca^{2+} did not form a dominant crystalline mineral phase in this system. However, because EDS mainly provides information on local elemental distribution, it remains insufficient to determine whether trace amounts of Ca^{2+} were incorporated into the struvite lattice.

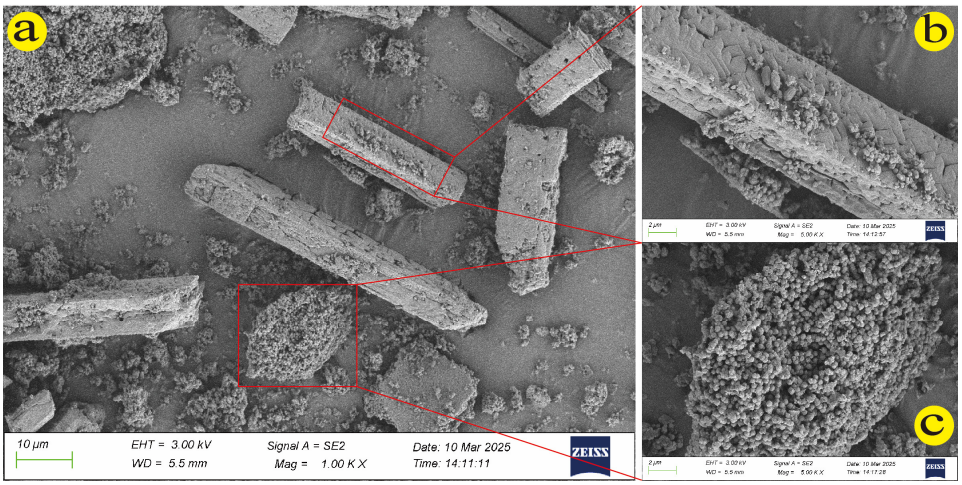

Figure 4. SEM images of precipitates formed during biomineralization with immobilized bacteria (**a**) and corresponding enlarged images (**b**,**c**).

In addition to regular struvite crystals, flocculent or aggregated deposits were also observed by SEM (Figure 4c). These deposits exhibited enrichment of Mg, Ca, P, and O ac-

cording to EDS analysis, but their elemental distributions were relatively diffuse (Figure S3). Such structures may consist of inorganic ions associated with biological organic components and may also contain poorly crystalline mineral precipitates. Since temporal changes in mineral phases during biomineralization were not investigated, these aggregated deposits cannot be conclusively identified as amorphous precursors of struvite formation based solely on endpoint SEM-EDS observations. These findings further suggest that phosphorus removal in the liquid phase involves not only crystalline struvite formation but also interfacial interactions between biological organic components and inorganic ions.

3.2.3. FTIR and TG-DTA Analyses

In the FTIR spectra (Figure 5a), the characteristic stretching vibration peak of PO_4^{3-} was observed at approximately 1013 cm^{-1}, while the corresponding bending vibrations appeared in the range of 570–463 cm^{-1}. The absorption peaks around 883, 762, and 700 cm^{-1} were also consistent with the reported characteristic peaks of struvite [8,17,21], further confirming that struvite was the predominant inorganic phase in the precipitates. The broad peak near 3285 cm^{-1} was associated with hydroxyl groups or structural water [12], whereas the absorption bands around 1655, 1543, and 1439 cm^{-1} indicated the presence of organic components in the samples. These results were consistent with the SEM observations of cellular structures and organic deposits on crystal surfaces, suggesting that the minerals formed in cultures containing IBMs retained typical bio-organic–inorganic composite characteristics.

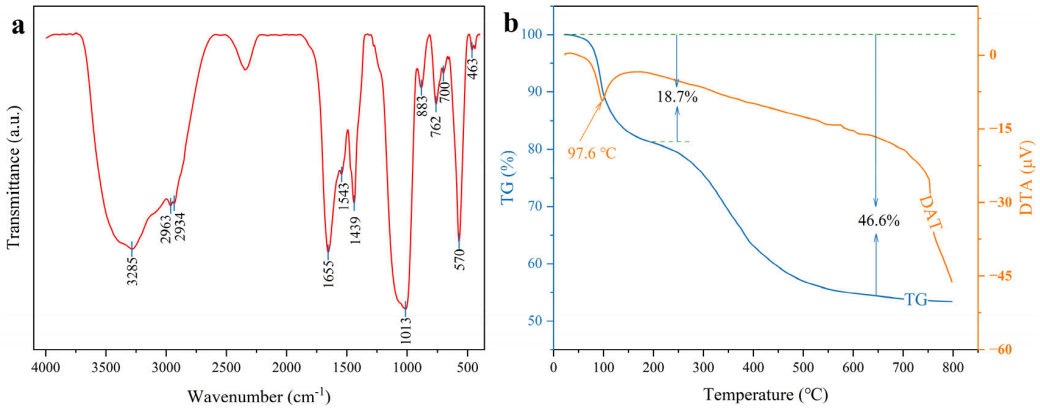

Figure 5. FTIR spectra (**a**) and TG-DTA analysis (**b**) of recovered struvite.

The TG-DTA results showed two major weight-loss stages in the samples (Figure 5b). The first stage occurred from room temperature to approximately 200 °C, with a weight loss of about 18.7% and an evident endothermic peak at approximately 97.6 °C, which was mainly attributed to the release of adsorbed water, partial structural water, and thermally unstable components. A further weight loss of approximately 27.9% occurred between 200 and 750 °C, which may have involved the release of crystal water from struvite, NH_3 volatilization, and decomposition of biological organic components. Because these processes partially overlap within this temperature range, the contributions of individual organic and inorganic components cannot be accurately distinguished solely based on thermal analysis. Collectively, the FTIR and TG-DTA results indicate that the struvite produced in the immobilized system not only possessed typical inorganic structural characteristics but also retained detectable biological organic components, further demonstrating the bio-organic–inorganic composite nature of the biomineralization products. Future studies combining time-resolved mineralogical characterization and detailed analysis of organic

components will help clarify the potential regulatory roles of biological organic matter during struvite nucleation and crystal growth.

3.2.4. Specific Surface Area and Pore Size Characteristics

The pore structure and pore size distribution of the struvite produced in the immobilized system are shown in Figure 6. The struvite exhibited an obvious adsorption–desorption hysteresis loop. According to the IUPAC classification, the adsorption isotherm displayed a type IV characteristic accompanied by an H3 hysteresis loop ($P/P° > 0.4$), indicating the presence of a mesoporous structure in the recovered struvite [22]. BET analysis revealed that the specific surface area of the struvite reached 168.71 m^2/g, which was substantially higher than that of biogenic struvite previously synthesized using $MgCl_2$ as the magnesium source (45.4721 m^2/g) [23], and also exceeded that of struvite produced by free LB002 using seawater-derived Mg^{2+} (140.9718 m^2/g) [6]. It should be emphasized that the numerical comparisons above were derived from separate experiments, and no synchronous parallel free-cell control was included in the present study. Therefore, the relatively high specific surface area observed here cannot be directly attributed to the immobilization treatment itself. Rather, these results simply indicate that the recovered struvite possessed a relatively large specific surface area and a pronounced mesoporous structure, providing a material basis for further evaluation of its interfacial reactivity and Cd^{2+} immobilization potential.

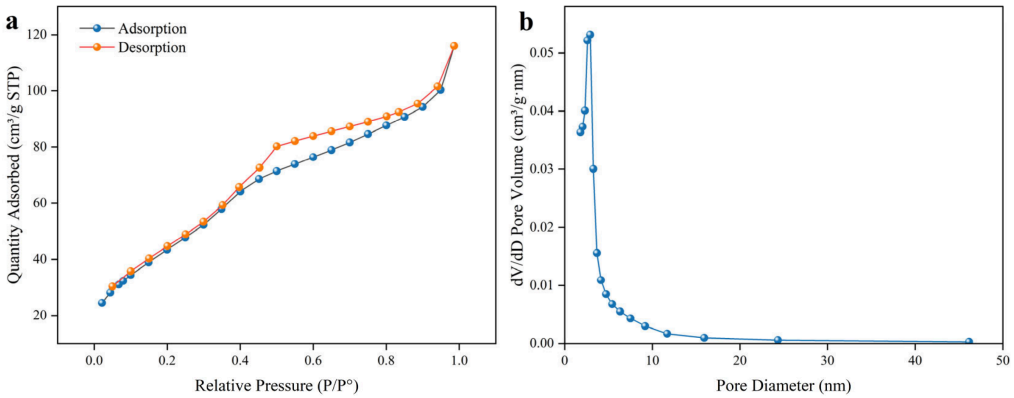

Figure 6. N_2 adsorption–desorption isotherm (**a**) and pore size distribution (**b**) of recovered struvite.

3.3. Repeated Phosphorus Recovery Performance of Immobilized LB002

Beyond mineralogical characteristics, the ability of the immobilized system to sustain biomineralization over repeated reuse cycles distinguishes this study from previous work using free bacteria. The temporal variations in TP and Mg^{2+} concentrations in the culture medium are shown in Table 1 and Figure S4.

Table 1. Key parameters during struvite biomineralization and reuse of immobilized bacteria.

Treatment	Struvite Yield (g/L)	Percent Removal of TP (%)	Percent Recovery of TP (%)	Mg^{2+} Transformation Efficiency (%)
IB	1.43 ± 0.063	98.26 ± 0.027	54.72 ± 2.42	12.53 ± 0.55
IB-I	1.38 ± 0.11	97.07 ± 0.36	52.60 ± 4.11	12.05 ± 0.94
IB-II	1.40 ± 0.077	97.54 ± 0.023	53.43 ± 2.96	12.24 ± 0.68
IB-III	1.31 ± 0.062	95.84 ± 0.32	50.06 ± 2.38	11.47 ± 0.54

Note: IB represents the initial biomineralization treatment with immobilized bacteria; IB-I, IB-II, and IB-III represent the first, second, and third reuse cycles of immobilized bacteria after recovery, respectively. Data are presented as mean ± SD (n = 3).

During the initial biomineralization cycle, the TP concentration in the culture medium decreased from 10.94 mmol/L to 0.19 mmol/L, corresponding to a TP removal of 98.26%. Meanwhile, the Mg^{2+} transformation efficiency reached 12.53%, the struvite yield was 1.43 g/L, and the TP recovery efficiency in the form of struvite was 54.72%. These results were comparable to those obtained from the previous free LB002 seawater-based system, which achieved a TP removal efficiency of 98.30% and a phosphorus recovery efficiency of 55.06%, indicating that immobilization did not impair the ability of LB002 to induce seawater-derived Mg^{2+}-driven struvite biomineralization.

After recovery, the IBMs were reused continuously for three additional biomineralization cycles (IB-I, IB-II, and IB-III). The TP removal efficiencies were 97.07%, 97.54%, and 95.84%, respectively, demonstrating that the system maintained high phosphorus removal capacity during repeated operation. Correspondingly, the struvite yield decreased only slightly from 1.43 g/L in the initial cycle to 1.38, 1.40, and 1.31 g/L in subsequent cycles. Similar trends were observed for TP recovery efficiency and Mg^{2+} transformation efficiency, which remained at 50.06% and 11.47%, respectively, after the third reuse cycle. These results demonstrate that the recovered and washed IBMs could be repeatedly transferred into fresh medium and maintained relatively stable biomineralization performance over three reuse cycles.

Although TP removal remained above 95% throughout all reuse cycles, the phosphorus recovery in the form of struvite was only approximately 50%, indicating that not all phosphorus removed from the liquid phase was recovered as struvite. In addition to struvite formation, a fraction of the phosphorus may have been retained through microbial assimilation, association with cell surfaces or extracellular polymeric substances (EPS), or incorporation into other poorly crystalline, amorphous, or fine particulate phosphorus-containing precipitates. However, these individual phosphorus pools were not independently quantified in the present study; therefore, a complete phosphorus mass balance could not be established, and the relative contributions of different phosphorus sinks could not be determined. Future studies should separately quantify phosphorus in the liquid phase, cell-associated and bio-organic fractions, and different mineral phases to establish a more complete phosphorus mass balance and improve the quantitative assessment of phosphorus recovery efficiency in this system. After the third reuse cycle, visible breakage of some IBMs was observed (Figure S5). However, the system still maintained a TP removal efficiency of 95.84% and a phosphorus recovery efficiency of 50.06%, suggesting that the mineralization function of LB002 was not substantially impaired despite structural damage to the carrier. Therefore, the primary limitation for extending the operational lifespan of the immobilized system may gradually shift from microbial mineralization activity to the structural stability of the microspheres. During long-term operation, PVA–SA immobilization materials may undergo swelling, changes in pore structure, and reduced mechanical strength due to continuous shaking, ion exchange, and microbial growth, ultimately resulting in particle breakage [11]. For future continuous operation systems, improving the swelling resistance and shear resistance of the carrier may be more critical than further increasing TP removal efficiency in a single cycle. With further optimization of carrier stability and reactor operating conditions, this system may provide a basis for developing continuous or repeated-batch seawater-derived magnesium-based phosphorus recovery processes, contributing to stable phosphorus removal and resource recovery from eutrophic coastal waters.

3.4. Cd^{2+} Adsorption Capacity of Struvite

The struvite produced by immobilized bacteria exhibited a high specific surface area and a pronounced mesoporous structure. Therefore, Cd^{2+} was selected as a representative

heavy metal to further evaluate its adsorption performance. The Langmuir model provided a good fit to the Cd^{2+} adsorption isotherm data, with a coefficient of determination (R^2) of 0.9955 and a predicted maximum adsorption capacity (Q_{max}) of 446.43 mg/g (Figure 7). This value was higher than the 386.10 mg/g reported for struvite produced by free LB002 in a seawater-based system [6] and also exceeded the 282.96 mg/g reported by Wang et al. [12]. However, because these values were obtained in different experiments rather than from a synchronous free-cell–immobilized-cell comparison, the higher value observed in the present study cannot be specifically attributed to bacterial immobilization. The relatively large specific surface area of the recovered struvite provides abundant accessible interfaces and may contribute to its apparent Cd^{2+} immobilization capacity. These characteristics further suggest that the recovered struvite has potential as a secondary functional material for the sequestration and removal of heavy metals from contaminated waters. It should be noted that the mechanisms underlying Cd^{2+} immobilization were not directly resolved in the present study. Previous studies have suggested that, in addition to surface adsorption, Cd^{2+} immobilization by biogenic struvite may involve surface functional-group complexation, ion exchange, mineral phase transformation, and the formation of Cd-containing phosphate phases [12,23]. Residual cellular components and EPS associated with biomineralization may also provide additional binding sites for Cd^{2+} [24]. These potential mechanisms are based on previous studies, and their relative contributions cannot be distinguished from the present adsorption isotherm data alone.

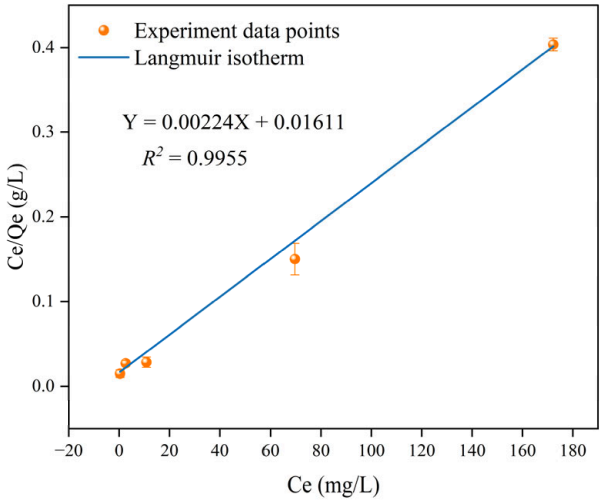

Figure 7. Langmuir model fitting of Cd^{2+} adsorption by the recovered struvite.

From the perspective of pollutant remediation, the Cd^{2+} immobilization capacity of the recovered phosphorus mineral indicates that struvite may serve not only as a carrier for phosphorus resource recovery but also as a secondary functional material for heavy-metal pollution control, thereby enhancing the overall resource utilization value of the biomineralization process. Future studies combining mineralogical characterization before and after adsorption with analyses of surface chemical states and biological organic components will help further elucidate the mechanisms of Cd^{2+} immobilization by biogenic struvite and clarify the potential roles of biological organic components in Cd^{2+} binding and mineral–solution interfacial reactions.

Taken together, immobilized LB002 combined with Mg^{2+} supplied by natural seawater supported microbially driven alkalization, struvite formation, and phosphorus recovery under the tested laboratory conditions. The IBMs were able to sustain struvite formation under high-salinity and complex ionic conditions and maintained relatively stable TP removal and phosphorus recovery over three consecutive reuse cycles. In addition, the recovered struvite

exhibited a high Cd^{2+} adsorption potential, indicating its potential application in downstream pollutant treatment and purification. Meanwhile, the breakage of the microspheres after the third cycle indicates that the mechanical stability of the carrier remains a major constraint on long-term operation. It should also be noted that the present study was conducted using a laboratory-prepared batch medium and did not include a synchronous parallel comparison between free and immobilized cells. Therefore, the effects of immobilization on salt tolerance, biomineralization kinetics, mineral properties, and Cd^{2+} immobilization cannot be quantitatively isolated. In addition, a complete phosphorus mass balance was not established. Future studies should address these limitations through direct free-cell–immobilized-cell comparisons, quantitative phosphorus partitioning, evaluation of bacterial loading on activated carbon and its contribution to immobilization performance, improved carrier design, continuous-flow experiments, and validation using actual eutrophic waters.

4. Conclusions

In this study, a reusable immobilized bacterial system was developed for struvite biomineralization using seawater as the magnesium source to achieve repeated phosphorus recovery. Immobilized LB002 continuously metabolized nitrogen-containing organic compounds, promoted NH_4^+ accumulation and alkalization of the system, and utilized seawater-derived Mg^{2+} to form struvite with high phase purity. In the initial cycle, TP removal and recovery efficiencies reached 98.26% and 54.72%, respectively, with a struvite yield of 1.43 g/L. After three consecutive reuse cycles, TP removal and recovery efficiencies remained at 95.84% and 50.06%, respectively, demonstrating relatively stable repeated phosphorus recovery performance. Although partial breakage of the microspheres was observed after the third cycle, biomineralization efficiency remained high, indicating that the mechanical stability of the carrier may be a major factor limiting further extension of the operational lifespan. The recovered struvite had a specific surface area of 168.71 m^2/g and a maximum Cd^{2+} adsorption capacity of 446.43 mg/g under the tested conditions. This study advances seawater-derived magnesium-based struvite biomineralization from a single-batch process using free bacteria to a reusable immobilized system, offering a new approach for sustained phosphorus recovery and the further valorization of biomineralization products. Future work should focus on improving carrier stability, clarifying phosphorus partitioning and Cd^{2+} immobilization mechanisms, and evaluating long-term performance in continuous-flow systems and real waters.

Supplementary Materials: The following supporting information can be downloaded at https://www.mdpi.com/article/10.3390/separations13100304/s1, Figure S1: Immobilized bacterial microspheres (a), and the N_2 adsorption–desorption isotherm (b) and pore size distribution (c) of activated carbon used as the immobilization carrier; Figure S2: EDS elemental mapping of struvite formed during biomineralization with immobilized bacteria; Figure S3: EDS elemental mapping of clustered deposits in the precipitates; Figure S4: Temporal variations in TP and Mg^{2+} concentrations in the culture medium during biomineralization by immobilized bacteria; Figure S5: Morphology of broken immobilized bacterial microspheres after the IB-III treatment and bacterial secretions attached to their surfaces; Table S1: Chemical composition of seawater.

Author Contributions: Conceptualization, L.M. and B.L.; methodology, L.M.; software, L.M.; investigation, L.M.; resources, B.L.; data curation, L.M.; writing—original draft preparation, L.M.; writing—review and editing, L.M. and B.L.; supervision, B.L.; project administration, B.L.; funding acquisition, B.L. All authors have read and agreed to the published version of the manuscript.

Funding: This research was funded by the National Natural Science Foundation of China (grant number 92351302) and the Science and Technology Support Plan of Guizhou Province (grant number 2023-145).

Data Availability Statement: Data is contained within the article or Supplementary Materials.

Conflicts of Interest: The authors declare no conflicts of interest.

Abbreviations

The following abbreviations are used in this manuscript:

IBMs	immobilized bacterial microspheres
EPS	extracellular polymeric substances
TP	total phosphorus
LB	Luria–Bertani
PVA	polyvinyl alcohol
SA	sodium alginate
XRD	X-ray diffractometer
SEM	scanning electron microscopy
EDS	energy-dispersive spectroscopy
FTIR	fourier-transform infrared spectroscopy
TG-DTA	thermogravimetric–differential thermal analysis

References

1. Cloern, J.E.; Abreu, P.C.; Carstensen, J.; Chauvaud, L.; Elmgren, R.; Grall, J.; Greening, H.; Johansson, J.O.R.; Kahru, M.; Sherwood, E.T.; et al. Human activities and climate variability drive fast-paced change across the world's estuarine–coastal ecosystems. *Glob. Change Biol.* **2015**, *22*, 513–529. [CrossRef] [PubMed]
2. Malone, T.C.; Newton, A. The globalization of cultural eutrophication in the coastal ocean: Causes and consequences. *Front. Mar. Sci.* **2020**, *7*, 670. [CrossRef]
3. Suresh, K.; Tang, T.; van Vliet, M.T.H.; Bierkens, M.F.P.; Strokal, M.; Sorger-Domenigg, F.; Wada, Y. Recent advancement in water quality indicators for eutrophication in global freshwater lakes. *Environ. Res. Lett.* **2023**, *18*, 63004. [CrossRef]
4. Reinhard, C.T.; Planavsky, N.J.; Gill, B.C.; Ozaki, K.; Robbins, L.J.; Lyons, T.W.; Fischer, W.W.; Wang, C.; Cole, D.B.; Konhauser, K.O. Evolution of the global phosphorus cycle. *Nature* **2016**, *541*, 386–389. [CrossRef] [PubMed]
5. Guan, Q.; Li, Y.; Zhong, Y.; Liu, W.; Zhang, J.; Yu, X.; Ou, R.; Zeng, G. A review of struvite crystallization for nutrient source recovery from wastewater. *J. Environ. Manag.* **2023**, *344*, 118383. [CrossRef] [PubMed]
6. Meng, L.; Lian, B. Bacterially induced synthesis of struvite under seawater stress: Characteristics and application potential. *J. Environ. Manag.* **2026**, *402*, 129060. [CrossRef] [PubMed]
7. Bradford-Hartke, Z.; Razmjou, A.; Gregory, L. Factors affecting phosphorus recovery as struvite: Effects of alternative magnesium sources. *Desalination* **2021**, *504*, 114949. [CrossRef]
8. Han, Z.; Guo, N.; Yan, H.; Xu, Y.; Wang, J.; Zhao, Y.; Zhao, Y.; Meng, L.; Chi, X.; Zhao, H.; et al. Recovery of phosphate, magnesium and ammonium from eutrophic water by struvite biomineralization through free and immobilized *Bacillus cereus* MRR2. *J. Clean. Prod.* **2021**, *320*, 128796. [CrossRef]
9. Liang, B.; Gao, D.; Munir, M.T.; Yu, W.; Wu, X.; Huang, Y.; Li, H.; Young, B.; Zhou, S.; Li, B. Struvite biomineralization as a promising solution to break the pollutant-resource paradox of phosphorus. *Chem. Eng. J.* **2024**, *493*, 152437. [CrossRef]
10. Yan, H.; Han, Z.; Zhao, H.; Pan, J.; Zhao, Y.; Tucker, M.E.; Zhou, J.; Yan, X.; Yang, H.; Fan, D. The bio-precipitation of calcium and magnesium ions by free and immobilized *Lysinibacillus fusiformis* DB1-3 in the wastewater. *J. Clean. Prod.* **2020**, *252*, 119826. [CrossRef]
11. Yan, H.; Cao, J.; Teng, M.; Meng, L.; Zhao, L.; Chi, X.; Han, Z.; Tucker, M.E.; Zhao, H. Calcium ion removal at different sodium chloride concentrations by free and immobilized halophilic bacteria. *Water Res.* **2023**, *229*, 119438. [CrossRef] [PubMed]
12. Wang, X.; He, X.; Xia, D.; Sun, M.; An, X.; Lian, B. The phase transformation of microbial induced struvite and its Cd(II) immobilization mechanism. *J. Environ. Chem. Eng.* **2022**, *10*, 107695. [CrossRef]
13. Sinha, A.; Singh, A.; Kumar, S.; Khare, S.K.; Ramanan, A. Microbial mineralization of struvite: A promising process to overcome phosphate sequestering crisis. *Water Res.* **2014**, *54*, 33–43. [CrossRef] [PubMed]
14. Zhang, P.; Ding, Y.; Zhao, T.; Wang, Y.; Yao, Q.; Fu, S.; Zhou, G. Can phosphobacteria simultaneously achieve phosphorus recovery and Pb^{2+} removal from wastewater by biomineralization? *Chem. Eng. J.* **2023**, *455*, 140734. [CrossRef]
15. Li, X.; He, X.; Ren, K.; Dong, H.; Lian, B. Mechanisms of carbonate precipitation induced by two model bacteria. *Chem. Geol.* **2023**, *628*, 121461. [CrossRef]
16. de Souza Meira, R.C.; Paz, S.P.A.D.; Corrêa, J.A.M. XRD-Rietveld analysis as a tool for monitoring struvite analog precipitation from wastewater: P, Mg, N and K recovery for fertilizer production. *J. Mater. Res. Technol.* **2020**, *9*, 15202–15213. [CrossRef]

17. Li, H.; Zhao, T.; Qian, F.; Jiang, H.; Yao, Q.; Luo, Y.; Fu, S.; Zhou, G. A model of extracellular polymeric substances on crystal growth and morphogenesis of struvite: Effects of sodium alginate. *Powder Technol.* **2021**, *380*, 80–88. [CrossRef]
18. Battaz, S.; Djazi, F.; Allal, H.; Trabelsi, I.; Abdellah, Z.; Benrabaa, R.; Hamzaoui, A.H. Phosphorus recovery as struvite from wastewater by using seawater, brine and natural brine. *Desalin. Water Treat.* **2024**, *317*, 100082. [CrossRef]
19. Kumari, S.; Jagadevan, S. Phosphorus recovery from municipal wastewater through struvite biomineralization using model gram-negative and gram-positive bacterial strains. *J. Clean. Prod.* **2022**, *366*, 132992. [CrossRef]
20. Zhao, T.; Li, H.; Jiang, H.; Yao, Q.; Huang, Y.; Zhou, G. Morphogenesis and evolution mechanisms of bacterially-induced struvite. *Sci. Rep.* **2021**, *11*, 170. [CrossRef] [PubMed]
21. Luo, Y.; Li, H.; Huang, Y.; Zhao, T.; Yao, Q.; Fu, S.; Zhou, G. Bacterial mineralization of struvite using MgO as magnesium source and its potential for nutrient recovery. *Chem. Eng. J.* **2018**, *351*, 195–202. [CrossRef]
22. Liu, R.; Lian, B. Immobilisation of Cd(II) on biogenic and abiotic calcium carbonate. *J. Hazard. Mater.* **2019**, *378*, 120707. [CrossRef] [PubMed]
23. Wang, X.; Meng, L.; Hu, M.; Gao, L.; Lian, B. The competitive and selective adsorption of heavy metals by struvite in the Pb(II)-Cd(II)-Zn(II) composite system and its environmental significance. *Water Res.* **2024**, *250*, 121087. [CrossRef] [PubMed]
24. Meng, L.; Lian, B. Bacterially induced synthesis of low-Cd struvite coupled with Cd^{2+} biosorption under high cadmium stress. *RSC Adv.* **2026**, *16*, 55952–55963. [CrossRef] [PubMed]

Disclaimer/Publisher's Note: The statements, opinions and data contained in all publications are solely those of the individual author(s) and contributor(s) and not of MDPI and/or the editor(s). MDPI and/or the editor(s) disclaim responsibility for any injury to people or property resulting from any ideas, methods, instructions or products referred to in the content.